

# Quadrupole-octupole coupling and the onset of octupole collectivity

Kosuke Nomura<sup>1,2,\*</sup>

<sup>1</sup>Department of Physics, Hokkaido University, Sapporo 060-0810, Japan

<sup>2</sup>Nuclear Reaction Data Center, Hokkaido University, Sapporo 060-0810, Japan

**Abstract.** Octupole deformation and collective excitations are studied within the interacting boson model. By using the results of the self-consistent mean-field calculations with a universal energy density functional, the Hamiltonian of the interacting  $s$ ,  $d$ , and  $f$  boson system is completely determined. A global systematic study confirms that significant octupole effects are present in actinide, lanthanide, and rare-earth nuclei corresponding to particular nucleon numbers for which octupole correlations are empirically suggested to be enhanced.

## 1 Introduction

In addition to the quadrupole deformation, the octupole correlations play roles in determining nuclear structure. The octupole correlations are enhanced in those nuclei with specific neutron  $N$  or/and proton  $Z$  numbers, i.e., 34, 56, 88, 134, . . . Search for the octupole deformed nuclei has been a topic of great interest for experimental and theoretical studies (see, e.g., [1] for a review). Observables that characterize the octupole collectivity are the low-lying negative-parity band, which forms an approximate alternating parity band with the positive-parity ground-state band, and the large  $E1$  and  $E3$  transition matrices connecting the bands. Experiments using radioactive-ion beams have confirmed evidence for a stable octupole shape in a number of nuclei in light actinide and lanthanide regions. Corresponding theoretical calculations have been reported by many authors using various nuclear structure models.

The interacting boson model (IBM) [2] has been successful in describing low-energy collective excitations in medium-heavy and heavy nuclei over a wide range of the nuclear chart. The assumption of the IBM is that correlated pairs of valence nucleons with spin  $0^+$  and  $2^+$  are represented by a  $s$  boson, and a  $d$  boson, respectively. To compute negative-parity states, including those arising from the octupole correlations, one should introduce in the IBM space octupole,  $f$  (spin  $3^-$ ), bosons. Note that the IBM itself is a phenomenological model, that is, the parameters have to be obtained from experiment. It should be, therefore, founded on the underlying multi-nucleon dynamics, so that the model Hamiltonian be derived from more fundamental nuclear structure models [3–5]. In particular, a mapping technique has been developed [5] that establishes the link between the IBM and the framework of energy density functional (EDF) for nuclear many-body systems [6–8]. This method consists in using the results of the self-consistent mean-field (SCMF) calculations based on a

university EDF to completely determine the IBM Hamiltonian, which is then used to calculate excitation spectra and transition properties.  $f$  bosons have also been considered in the mapping procedure [9, 10], which has allowed to study octupole deformations and collective excitations in a number of mass regions (see, [11], for a review).

This contribution presents recent results concerning the octupole collectivity, that are obtained from the IBM calculations based on the nuclear EDF. A brief overview of the SCMF-to-IBM mapping is given in Sec. 2. A global study of octupole collectivity in a large number nuclei (Sec. 3), and applications to a couple of more challenging cases that also involve effects of shape coexistence (Sec. 4) are presented. The results presented below are based on the works originally published in Refs. [10–18].

## 2 Theoretical framework

Within the EDF framework one often starts with the SCMF calculations with constraints on multipole moments, e.g., quadrupole, octupole, etc., to obtain total mean-field energy [hereafter denoted as potential energy surface (PES)] that is defined in terms of the intrinsic deformation variables. As an example, Fig. 1 shows the PES plotted as a function of the axially symmetric quadrupole ( $\beta_2$ ) and octupole ( $\beta_3$ ) deformations for the nucleus  $^{226}\text{Th}$ . The PES is here calculated within the constrained relativistic Hartree-Bogoliubov (RHB) approach employing the density-dependent point-coupling (DD-PC1) EDF [19] and the separable pairing force of finite range [20]. One should see from Fig. 1 a distinct, octupole-deformed global minimum at  $(\beta_2, \beta_3) \approx (0.2, 0.15)$ . Also shown in Fig. 1 is the projection of the calculated total nucleon intrinsic density onto the  $x$  and  $z$  plane of the intrinsic frame, corresponding to the  $\beta_2$  and  $\beta_3$  deformations giving the global minimum. The density distribution indeed takes on a pear-like shape.

The corresponding excited states are studied within the IBM. Here a version of the IBM that comprises  $s$ ,  $d$ , and

\*e-mail: nomura@sci.hokudai.ac.jp

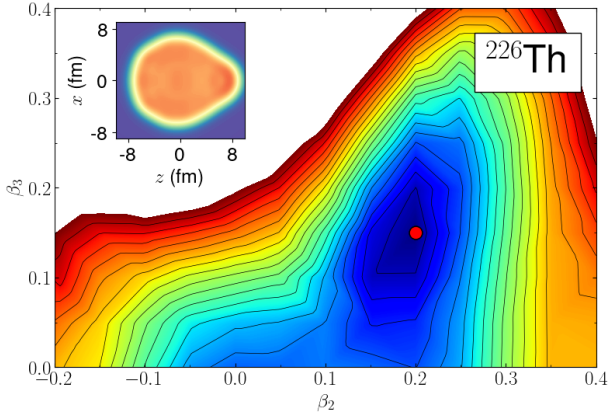


**Figure 1.** Axially-symmetric quadrupole  $\beta_2$  - octupole  $\beta_3$  SCMF PES, and total intrinsic density of  $^{226}\text{Th}$ , computed with the constrained RHB method using the DD-PC1 EDF and the separable pairing force of finite range. Energy difference between neighboring contours is 0.5 MeV. The red dot stands for the global minimum.

$f$  bosons (denoted as  $sdf$ -IBM) is considered, with the Hamiltonian expressed in general as

$$\hat{H} = \hat{H}_{sd} + \hat{H}_f + \hat{V}_{sd-f}, \quad (1)$$

where the first, second, and third terms on the right-hand side stand for the Hamiltonians composed of  $s$  and  $d$ , and of  $f$  bosons, and the interaction representing the coupling between the  $sd$ - and  $f$ -boson spaces, respectively. For each nucleus, parameters of the Hamiltonian (1) are determined by mapping the SCMF PES,  $E_{\text{SCMF}}(\beta_2, \beta_3)$ , onto the equivalent one in the IBM,  $E_{\text{IBM}}(\beta_2, \beta_3)$ , so that the equality

$$E_{\text{IBM}}(\beta_2, \beta_3) \approx E_{\text{SCMF}}(\beta_2, \beta_3), \quad (2)$$

is satisfied in the neighborhood of the global minimum. Note that  $E_{\text{IBM}}(\beta_2, \beta_3)$  is given as the energy expectation value taken in the coherent state [21] of  $s$ ,  $d$ , and  $f$  bosons. The mapped  $sdf$ -IBM Hamiltonian, with the parameters determined by the above procedure (2), is diagonalized in the Hilbert space spanned by  $n(= n_s + n_d + n_f)$  bosons. More thorough descriptions of the SCMF-to-IBM mapping procedure can be found in Refs. [10, 11].

Figure 2 depicts the ground-state band, consisting of positive-parity even-spin yrast states, and the band of negative-parity odd-spin yrast states of  $^{226}\text{Th}$ , obtained from the mapped  $sdf$ -IBM. The two bands appear to form a single band that resembles the alternating-parity band starting with spin  $I^\pi \approx 7^-$ . The excited  $0_2^+$  band is also predicted. The bandhead,  $0_2^+$  state, has been shown to be formed by the coupling between two  $f$  bosons. The  $0^+$  excited states of similar kind, which are interpreted as being of double octupole nature, have been predicted in other actinide nuclei [10]. It should be noted that the calculated bands from the mapped  $sdf$ -IBM are in a fairly good agreement with experiment, even though there is no phenomenological adjustment of the IBM parameters to ex-

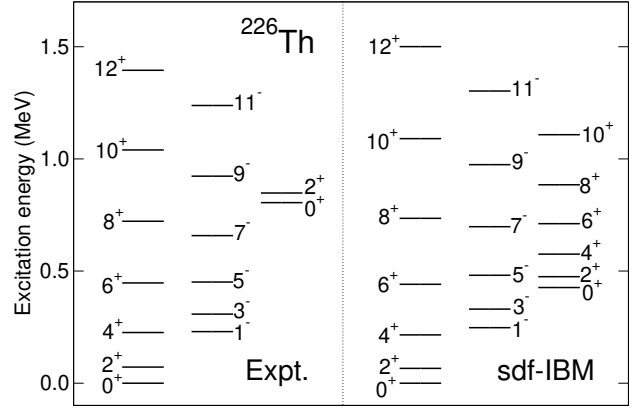


**Figure 2.** Experimental [22] (left) and predicted (right) low-energy spectra of  $^{226}\text{Th}$ .

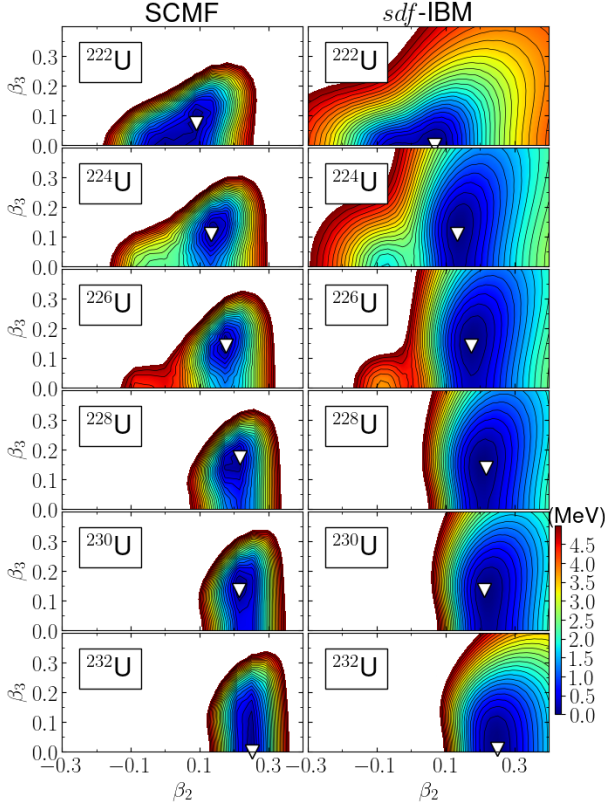
periment and the underlying EDF is not specifically tuned to produce octupole deformations.

### 3 Global study

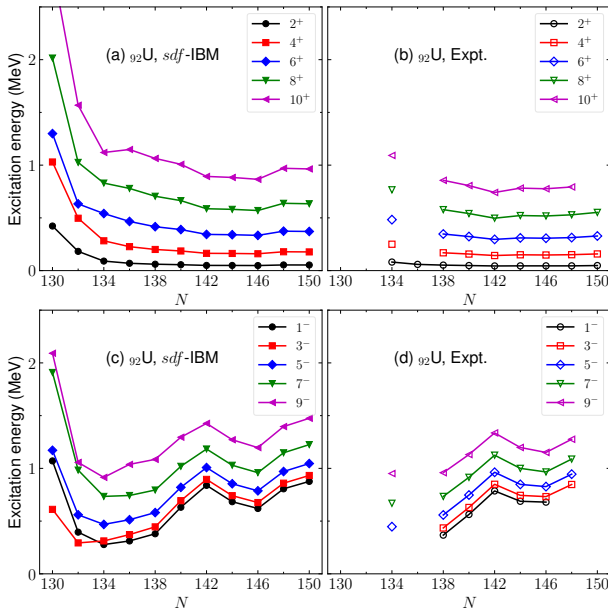
The actinide nuclei corresponding to  $N \approx 134$  and  $Z \approx 88$  within the mass range  $A = 200 - 250$  are among the best known for a stable octupole deformation and octupole collective excitations, the experimental evidence being, e.g.,  $^{220}\text{Rn}$ ,  $^{224}\text{Ra}$ , and  $^{226}\text{Th}$ . In that context, systematic studies on the even-even actinide nuclei in the isotopic chains from Ra ( $Z = 88$ ) to Cf ( $Z = 98$ ) have been performed [12, 13] within the mapped  $sdf$ -IBM with the microscopic input provided by the SCMF calculations based on the Gogny-type EDF. The discussion below concerns the U isotopes as an illustrative example.

Figure 3 shows, on the left-hand side, the SCMF  $\beta_2 - \beta_3$  PESs for the  $^{222-232}\text{U}$  nuclei obtained from the constrained Hartree-Fock-Bogoliubov (HFB) method [8] using the Gogny-D1M interaction [23], and the mapped  $sdf$ -IBM PESs on the right. While the magnitude of the quadrupole deformation remains almost constant, the octupole deformation appears to develop towards  $^{226}\text{U}$  or  $^{228}\text{U}$ , at which a pronounced minimum at  $\beta_3 \approx 0.2$  deformation is obtained. The potential, in turn, becomes softer in  $\beta_3$  direction for the nuclei heavier than the  $^{228}\text{U}$  isotope, and from  $^{232}\text{U}$  on, an octupole deformation is no longer observed. The same observation, that the nuclear shape evolves from the stable octupole to octupole-soft regimes, has been shown to apply to the neighboring isotopic chains, Ra, Th, Pu, Cm, and Cf [12, 13]. Another remark is that, comparing between the SCMF and IBM PESs for a given nucleus, the latter looks flat for larger  $\beta_2$  and  $\beta_3$  deformations. This is a general occurrence in the SCMF-to-IBM mapping procedure, and reflects the fact that the IBM has only limited degrees of freedom of valence nucleons only, whereas the SCMF model consists of all constituent nucleons.

Figure 4 compares the  $sdf$ -IBM and experimental low-lying even-spin positive-parity, and odd-spin negative-parity yrast states for the U isotopic chain. The



**Figure 3.** (Left column)  $\beta_2$ - $\beta_3$  SCMF PESs for the  $^{222-232}\text{U}$  isotopes computed by the constrained HFB method with the Gogny-D1M EDF. (Right column) mapped *sdf*-IBM PESs. The global minimum is indicated by the open triangle.



**Figure 4.** Low-energy spectra of the positive-parity even-spin (a), and negative-parity odd-spin (c) yrast states of the  $^{222-242}\text{U}$  isotopes calculated with the mapped *sdf*-IBM. Experimental data [22] are shown in (b,d). [22].

evolution of the positive-parity energy levels shown in Fig. 4(a) and 4(b) suggests a rapid transition from nearly spherical to strongly prolate deformed shapes around  $N = 132$ , and one can see a rotational-like band structure all the way until  $N = 150$ . The calculated negative-parity energy levels in Figs. 4(c) exhibit a parabolic dependence on  $N$  with minima around  $N = 134$ , at which the most pronounced octupole deformed ground state is obtained in the PES. These negative-parity levels increase in energy from  $N = 134$  to 142, but turns to decrease again, showing another parabolic behavior around  $N = 146$ , both in the calculation and experimentally [Fig. 4(d)]. The appearance of such a local behavior may point to the importance of dynamical octupole correlations in the heavier actinide nuclei around  $N = 146$ . This can be also inferred from the fact that, even though the PES does not have a non-zero  $\beta_3$  minimum for those nuclei with  $N \geq 140$ , the potential is soft in  $\beta_3$  deformation, hence indicating the considerable amount of fluctuation that could lower the negative-parity levels.

As well as in the actinide region, calculations using the mapped *sdf*-IBM framework based on the Gogny-D1M EDF have been performed for the isotopes in the neutron-deficient [16] and neutron-rich [15] lanthanide, and rare-earth [14] regions, corresponding to  $N/Z = 34, 56$ , and 88, in which octupole deformation is supposed to be stabilized. Figure 5 shows the computed excitation energies of the  $3_1^-$  state,  $E(3_1^-)$ , and  $B(E3) \equiv B(E3; 3_1^- \rightarrow 0_1^+)$  transition probabilities in comparison to the experimental data.

As one saw in Fig. 4 many of the actinide nuclei with  $N = 130 - 150$  exhibit a lowering of  $E(3_1^-)$  around  $N = 134$ . The corresponding  $B(E3)$  values in Fig. 5(c) show an inverse parabolic behavior with maximal values at  $N \approx 134$ . Another region of interest is the lanthanide and rare-earth nuclei corresponding to  $(N, Z) = (88, 56)$ , from the Xe ( $Z = 54$ ) up to Gd ( $Z = 64$ ) isotopes with  $N = 84 - 94$ . The Gogny-HFB SCMF calculations in [14, 15] have produced an octupole deformed ground state with small,  $\beta_3 \approx 0.1$  value, in the PESs for the Xe, Ba, Ce, Nd, Sm, and Gd nuclei with  $N \approx 88$ . Similar behavior of the calculated  $E(3_1^-)$  values is observed for these isotopes [see Fig. 5(a)]. Particularly low-lying  $3_1^-$  energy levels are obtained for the Ba and Ce isotopes. The description of the  $B(E3)$  values in these isotopes is generally good [see Figs. 5(c) and 5(d)].

Also in the neutron-deficient nuclei with  $N \approx Z \approx 56$ , the Gogny-D1M SCMF calculation in Ref. [16] suggested a few instances exhibiting an octupole mean-field minimum:  $^{112}\text{Ba}$ ,  $^{114}\text{Ba}$ , and  $^{114}\text{Ce}$ . As in the other mass regions, the *sdf*-IBM produces the  $E(3_1^-)$  and  $B(E3)$  values that exhibit parabolic dependencies on  $N$ . However, spectroscopic data on these neutron-deficient nuclei is very limited in this mass region, as it is rather close to the proton dripline.

## 4 Effects of shape coexistence

Octupole correlations should be present in those nuclei corresponding to  $(N, Z) \approx (34, 34)$ , and  $(56, 34)$  as well. Description of these nuclear systems is, however, even

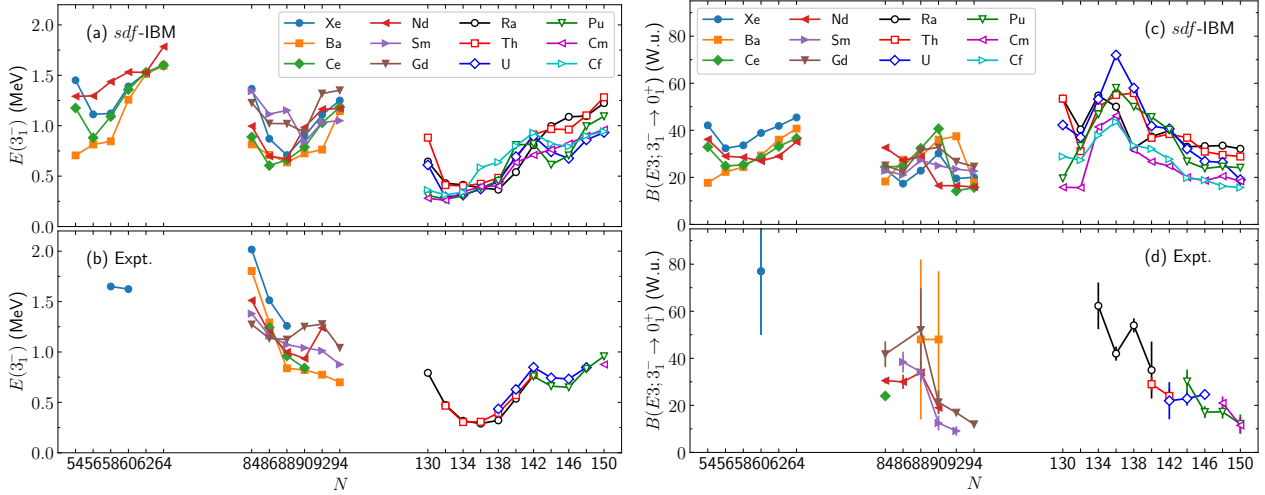


**Figure 5.** Calculated and observed excitation energies of the  $3_1^-$  states [panels (a) and (b)], and  $B(E3; 3_1^- \rightarrow 0_1^+)$  transition probabilities [panels (c) and (d)] for a series of isotopes.

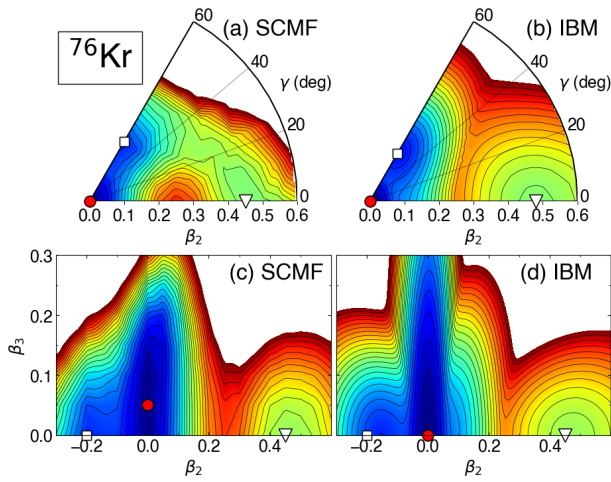


**Figure 6.** Triaxial quadrupole  $\beta_2 - \gamma$ , and axially-symmetric  $\beta_2 - \beta_3$  PESs for  $^{76}\text{Kr}$ . The SCMF PESs, obtained from the constrained RHB calculations using the DD-PC1 EDF and the separable pairing force of finite range [panels (a) and (c)], are compared with the mapped IBM PESs [panels (b) and (d)]. Energy difference between neighboring contours is 0.1 MeV. The spherical global minimum, oblate, and prolate local minima are represented by the solid circles, open squares, and triangles, respectively.

more challenging, as the octupole effects are to a large extent overshadowed by other shape degrees of freedom. Neutron-deficient  $N \approx Z \approx 34$  nuclei, for instance, present coexistence of prolate and oblate shapes, and also the triaxial deformation plays a role.

In Ref. [17] effects of shape coexistence in the low-energy quadrupole and octupole collective states in the neutron-deficient  $^{72}\text{Ge}$ ,  $^{74}\text{Se}$ , and  $^{74,76}\text{Kr}$  nuclei has been analyzed. For that purpose, the mapped *sdf*-IBM has been extended to include the configuration mixing of normal

and intruder states which are attributed to the emergence of shape coexistence. As an example, Fig. 6(a) depicts the SCMF PES with the triaxial quadrupole  $\beta_2 - \gamma$  deformations for  $^{76}\text{Kr}$ , obtained from the RHB method using the DD-PC1 EDF and the separable pairing force. There observed three minimum, a spherical global minimum, and two local minima on the oblate,  $\beta_2 \approx 0.25$ , and on the prolate,  $\beta_2 \approx 0.45$ , sides. The  $\beta_2 - \beta_3$  RHB PES is shown in Fig. 6(c). The global minimum appears at finite  $\beta_3$  deformation, even though the potential around the global minimum is shallow.

The appearance of the three different mean-field minima has been incorporated in the *sdf*-IBM in the following way. First, three independent *sdf*-IBM Hamiltonians consisting of  $n$ ,  $n + 2$ , and  $n + 4$  bosons are considered, which represent, respectively, the normal (0p-0h), and two-particle-two-hole (2p-2h), and four-particle-four-hole (4p-4h) intruder states [24]. The normal, 2p-2h, and 4p-4h Hamiltonians are then associated with the spherical global minimum, oblate, and prolate local minima, respectively. The Hamiltonian of the whole system consists of the three Hamiltonian, and the interactions that admix different configurations, and is diagonalized within the extended Hilbert space defined as the direct sum of the three subspaces. Figures 6(b) and 6(d) show, respectively, the mapped *sdf*-IBM PESs in the  $\beta_2 - \gamma$ , and  $\beta_2 - \beta_3$  planes, with the Hamiltonian completely determined by the SCMF calculations. For details, see Ref. [17].

Figure 7 compares the low-energy spectra for  $^{76}\text{Kr}$  between the *sdf*-IBM that includes only the single configuration associated with the spherical global minimum, and the *sdf*-IBM that takes into account the configuration mixing of the three boson subspaces associated with the spherical, oblate, and prolate mean-field minima. A significant impact of introducing the configuration mixing is that the excited  $0^+$  levels are dramatically lowered. The predicted  $K^\pi = 0_2^+$  and  $0_3^+$  bands are associated with the oblate 2p-

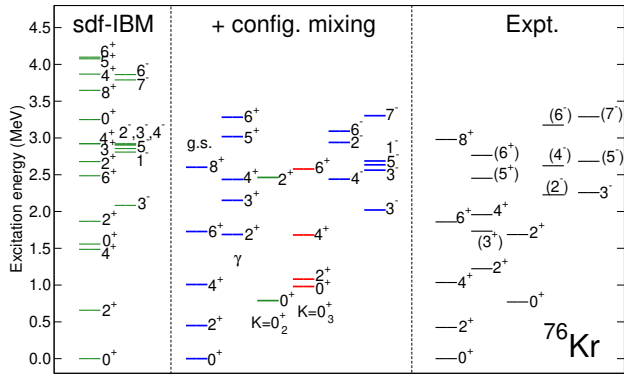


**Figure 7.** Calculated low-energy spectra for the  $^{76}\text{Kr}$  nucleus obtained from the *sdf*-IBM that does not (left panel) and does (middle panel) include the configuration mixing. The observed energy spectrum is shown on the right panel.

2h, and prolate 4p-4h configurations, respectively, while the ground-state (g.s.),  $\gamma$ , and negative-parity bands are of normal, 0p-0h one. The description of negative-parity levels is also improved by the inclusion of configuration mixing. Similar results have been obtained for neighboring isotopes,  $^{72}\text{Ge}$ ,  $^{74}\text{Se}$ , and  $^{74}\text{Kr}$  [17].

The mapped *sdf*-IBM has also been applied to the neutron-rich  $N \approx 56$  Se, Kr, Sr, Zr, and Mo isotopes [18]. The SCMF calculations using the RHB model with the DD-PC1 EDF, however, have not produced any octupole-deformed ground state even at  $N = 56$ . The corresponding *sdf*-IBM calculations provided the lowest negative-parity states at the excitation energies of  $\approx 1.5 - 2.0$  MeV, but failed in reproducing behaviors of positive-parity low-spin states in the Zr isotopes that exhibits an abrupt decrease of energy levels at  $N = 60$ . For the neutron-rich nuclei in this region, using only the axially symmetric  $\beta_2$  and  $\beta_3$  degrees of freedom may not be sufficient, and some other degree of freedom such as triaxiality may need to be considered, or the problem may well point to a certain deficiency of the underlying EDF.

## 5 Summary

Recent theoretical calculations on the quadrupole and octupole collective states in a large number of medium-heavy and heavy nuclei within the *sdf*-IBM that is based on the nuclear EDF have been presented. A global systematic study using this framework has confirmed many instances for enhanced octupole collectivity at those nuclei corresponding to the nucleon numbers 34, 56, 88, and 134, for which the octupole deformation has been observed. On

the other hand, it has been suggested that some higher-order effects, such as the coexistence of different intrinsic shapes, or additional shape degrees of freedom, e.g., quadrupole triaxial, tetrahedral, hexadecapole, etc. deformations, need to be incorporated in the SCMF-to-IBM mapping procedure for precise descriptions of the proton-rich  $N \approx Z \approx 34$ , and neutron-rich  $N \approx 56$  nuclei.

## References

- [1] P.A. Butler, *J. Phys. G* **43**, 073002 (2016).
- [2] F. Iachello and A. Arima, *The interacting boson model* (Cambridge University Press, Cambridge, 1987).
- [3] T. Otsuka, A. Arima, and F. Iachello, *Nucl. Phys. A* **309**, 1 (1978).
- [4] T. Mizusaki, and T. Otsuka, *Prog. Theor. Phys. Suppl.* **125**, 97 (1996).
- [5] K. Nomura, N. Shimizu, and T. Otsuka, *Phys. Rev. Lett.* **101**, 142501 (2008).
- [6] M. Bender, P.-H. Heenen, and P.-G. Reinhard, *Rev. Mod. Phys.* **75**, 121 (2003).
- [7] T. Nikšić, D. Vretenar, and P. Ring, *Prog. Part. Nucl. Phys.* **66**, 519 (2011).
- [8] L.M. Robledo, T.R. Rodríguez and R.R. Rodríguez-Guzmán, *J. Phys. G* **46**, 013001 (2019).
- [9] K. Nomura, D. Vretenar, and B.-N. Lu, *Phys. Rev. C* **88**, 021303(R) (2013).
- [10] K. Nomura *et al.*, *Phys. Rev. C* **89**, 024312 (2014).
- [11] K. Nomura, *Int. J. Mod. Phys. E* 2340001 (2023).
- [12] K. Nomura *et al.*, *Phys. Rev. C* **102**, 064326 (2020).
- [13] K. Nomura *et al.*, *Phys. Rev. C* **103**, 044311 (2021).
- [14] K. Nomura, R. Rodríguez-Guzmán, and L.M. Robledo, *Phys. Rev. C* **92**, 014312 (2015).
- [15] K. Nomura *et al.*, *Phys. Rev. C* **104**, 044324 (2021).
- [16] K. Nomura, R. Rodríguez-Guzmán, and L.M. Robledo, *Phys. Rev. C* **104**, 054320 (2021).
- [17] K. Nomura, *Phys. Rev. C* **106**, 024330 (2022).
- [18] K. Nomura, *Phys. Rev. C* **105**, 054318 (2022).
- [19] T. Nikšić, D. Vretenar, and P. Ring, *Phys. Rev. C* **78**, 034318 (2008).
- [20] Y. Tian, Z.Y. Ma, and P. Ring, *Phys. Lett. B* **676**, 44 (2009).
- [21] J.N. Ginocchio and M.W. Kirson, *Nucl. Phys. A* **350**, 31 (1980).
- [22] <http://www.nndc.bnl.gov>.
- [23] S. Goriely, S. Hilaire, M. Girod, and S. Péru, *Phys. Rev. Lett.* **102**, 242501 (2009).
- [24] P.D. Duval and B.R. Barrett, *Phys. Lett. B* **100**, 223 (1981).